Image Reconstruction and Enhancement for Subsurface Radar Imaging Using Wavefield Statistics

Michael Chang, Hua Lee, and Iwaki Akiyama

Department of Electrical and Computer Engineering
University of California, Santa Barbara, CA 93106

Abstract

Frequency Modulated, Continuous Wave (FM-CW) radar has many applications toward NDE of civil structures, as well as the imaging of buried objects. In this paper, we first introduce the theory behind the operation of stepped chirp FM-CW subsurface radar, and then present an image enhancement technique based on the wavefield statistics. The technique uses the second order statistics of the frequency-domain representation of each point in the output to clarify target peaks and reduce the magnitude of surrounding areas. Experimental results using FM-CW ground-penetrating radar on buried targets of varying depths are included to demonstrate the effectiveness of stepped chirp radar and the enhancement technique.

Introduction

The ability to image subsurface objects has been growing in importance for several decades. Frequency Modulated, Continuous Wave (FM-CW) radar provides an effective method for this application, such as locating hazardous waste storage containers and buried ordinance[1]. Other applications of FM-CW radar include NDE of civil structures, such as the detection of voids, cracks, and conditions of reinforcement bars in concrete[2, 3]. Subsurface imaging of civil structures also provides a means of evaluating the structural integrity of roadways, buildings, and bridges to confirm design specifications.

Subsurface stepped FM-CW radar illuminates a target at various frequencies and records the change in phase and amplitude of the return signal. Performing a Fourier Transform provides the range profile of the object of interest. This approach provides the depth profile since the original data is modelled as frequency samples and the resultant inverse transformed image has a range index directly proportional to the depth.

In this paper we present an enhancement technique which utilizes the differences in wavefield statistics when a target is present to heighten target peaks and improve resolution. Experiments are performed on buried targets with stepped FM-CW radar in monostatic imaging configurations to reconstruct subsurface profiles. We then apply the enhancement technique to the profiles in order to demonstrate the effectiveness of this method.

Image formation

A stepped FM-CW radar imaging system transmits an RF signal between a start frequency, f_0, and a stop frequency, f_{N-1}, in equal, linear increments. The radar continuously transmits at each step. The return signal is formed by mixing the received signal with a portion of the transmitted signal and low-pass filtering. The return signal is digitized at each frequency step and stored. After a complete sweep of all N frequencies, a Fast Fourier Transform (FFT) is performed on the stored data to form the range profile[4]. The range information is present mainly in the phase of the return signal, and is based on the phase difference between the received signal and the transmitted signal. In Fig. (1), a rough diagram of a stepped FM-CW system and the stepped FM technique are presented[4]. The transmitter and receiver are close enough compared to the distance to the targets to approximate a monostatic configuration. Two paths are traced, 2–3–4–5–6 and 7–8. There is a phase associated with each path, θ_{ext} and θ_{int}, respectively. The system is designed such that the path length 7–8 is the same as 2–3–5–6. Thus, when the trans-

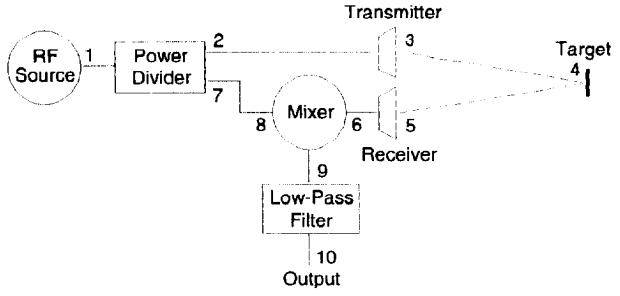

Figure 1. A stepped FM-CW system.

mitter is directly attached to the receiver (eliminating the external path length 3–4–5) the path lengths are equal and θ_{ext} equals θ_{int}. When a target is present, the path lengths are unequal, and a phase difference of ψ occurs. ψ can be expressed as:

$$\psi = \theta_{ext} - \theta_{int} = (2\pi f)\tau = (2\pi f)\frac{d}{c} \quad (1)$$

where f is the frequency of transmission (Hz), τ is the time of flight (the time required for the transmitted signal to reach the target and reflect back to the receiver, path 3–4–5), d is the round trip distance to the target (length of path 3–4–5), and c is the velocity of propagation of the signal in the medium[4].

When a single step frequency f_n is transmitted, the output of the mixer (path ending at 9) is:

$$v(n) = R_n cos(2\pi f_n t + \theta_{int}) cos(2\pi f_n t + \theta_{ext}) \quad (2)$$

where R_n is the amplitude of the return signal. Since $\theta_{ext} = \theta_{int} + \psi_n$ for a frequency f_n, we obtain:

$$\begin{aligned} v(n) &= R_n cos(2\pi f_n t + \theta_{int}) cos(2\pi f_n t + \theta_{int} + \psi_n) \\ &= \frac{R_n}{2} cos(\psi_n) + \frac{R_n}{2} cos(4\pi f_n t + 2\theta_{int} + \psi_n). \quad (3) \end{aligned}$$

After low-pass filtering, the output (path ending at 10) simply becomes[4]:

$$v(n) = \frac{R_n}{2} cos(\psi_n). \quad (4)$$

Since $\psi_n = (2\pi f_n)\frac{d}{c}$, ψ_n remains constant for a step frequency f_n. The step frequencies can be represented as:

$$f_n = f_0 + n\Delta f, \quad 0 \le n \le N-1 \quad (5)$$

where f_0 is the initial frequency, and Δf is the frequency step increment. Substituting into Eq. (4), we obtain:

$$\begin{aligned} v(n) &= \frac{R_n}{2} cos\left(2\pi f_n \frac{d}{c}\right) \\ &= \frac{R_n}{2} cos\left(2\pi \frac{d}{c}(f_0 + n\Delta f)\right) \\ &= \frac{R_n}{2} cos\left(2\pi \frac{d}{c} f_0 + \left(2\pi \frac{d\Delta f}{c}\right) n\right). \quad (6) \end{aligned}$$

If we define the constants $\phi_0 = 2\pi \frac{d}{c} f_0$ and $\phi = 2\pi \frac{d\Delta f}{c}$, the output can be expressed as a function of n:

$$v(n) = \frac{R_n}{2} cos(\phi_0 + \phi n), \quad 0 \le n \le N-1. \quad (7)$$

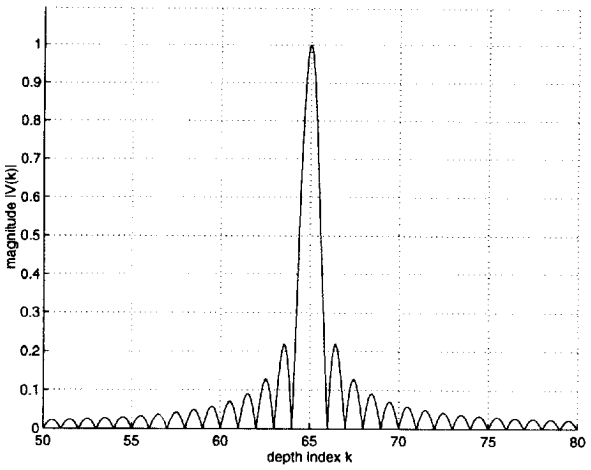

Figure 2. Typical range profile $|V(k)|$ with target at $k = 65$ and $|A| = 1$.

The type of modulation scheme used by the Ground-Penetrating Radar (GPR) system is actually Quadraphase Modulation[4]. The system also simultaneously mixes the received signal with a 90° shifted version of the transmitted signal, forming the Inphase and Quadrature components of the output:

$$\begin{aligned} v_1(n) &= \frac{R_n}{2} cos(\phi_0 + \phi n) \\ v_2(n) &= -\frac{R_n}{2} sin(\phi_0 + \phi n). \quad (8) \end{aligned}$$

Applying Euler's Theorem with $v_1(n)$ and $v_2(n)$ as the real and imaginary components of the output, we obtain:

$$v(n) = A_n e^{-j\phi n}, \quad 0 \le n \le N-1 \quad (9)$$

where A_n is defined as $A_n \equiv \frac{R_n}{2} e^{-j\phi_0}$.

An FFT is performed on $v(n)$ to form the range profile. We first make the assumption that $A_n \approx A$ for all n, where A is a constant (we assume the reflections at different frequencies have identical amplitudes). Then the output reduces to:

$$v(n) = Ae^{-j\phi n}, \quad 0 \le n \le N-1. \quad (10)$$

Performing an inverse FFT yields:

$$\begin{aligned} V(k) &= \frac{A}{N} \frac{sin\left[\pi\left(k - \frac{\phi N}{2\pi}\right)\right]}{sin\left[\frac{\pi}{N}\left(k - \frac{\phi N}{2\pi}\right)\right]} e^{j\left[\frac{\pi(N-1)}{N}\left(k - \frac{\phi N}{2\pi}\right)\right]}, \\ & 0 \le k \le N-1 \quad (11) \end{aligned}$$

where $V(k)$ = inverse FFT$\{v(n)\}$. If only the magnitude of the range profile is displayed, this reduces to:

$$|V(k)| = \frac{|A|}{N} \frac{\left|sin\left[\pi\left(k - \frac{\phi N}{2\pi}\right)\right]\right|}{\left|sin\left[\frac{\pi}{N}\left(k - \frac{\phi N}{2\pi}\right)\right]\right|}, \quad 0 \le k \le N-1. \quad (12)$$

A general plot of $|V(k)|$ is provided in Fig. (2). The magnitude peaks sharply when the depth index $k \approx \frac{\phi N}{2\pi}$.

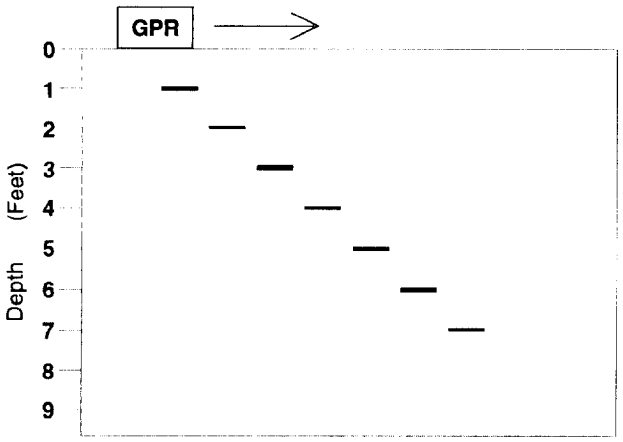

Figure 3. Cross-sectional view of test pit containing 7 metal plates.

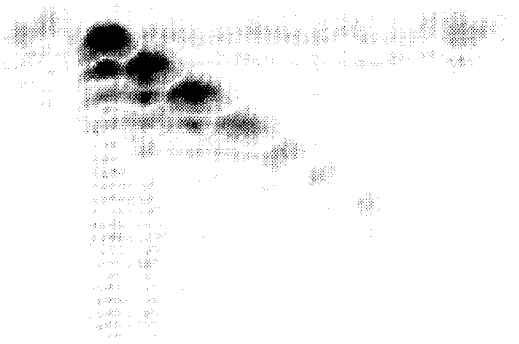

Figure 4. FFT formed image of 7 buried metal plates.

Since $\phi = 2\pi \frac{d\Delta f}{c}$, this is equivalent to:

$$k \approx \frac{Nd\Delta f}{c} = S\frac{d}{2} \tag{13}$$

where $S = \frac{2N\Delta f}{c}$ is a constant. Since d is the round trip distance to the target, we can express k as:

$$k \approx Sr \tag{14}$$

where $r = \frac{d}{2}$ is the one-way distance from the transmitter to the target. Thus the range index k is directly proportional to the depth of the range profile by the scaling factor S. When targets are closer, the peak in the magnitude of the range of the range profile moves to a correspondingly smaller value of k, and farther targets produce peaks at larger values of k.

The frequency range of the actual GPR used is 196–708 MHz for a bandwidth of 512 MHz. The frequencies are swept with steps of $\Delta f = 4$ MHz ($N = 128$). For the first experiment, 7 square metal plates (1 ft. $\times$ 1 ft.) were buried in a pit filled with plaster sand at various depths from 1 to 7 ft. deep. The seven metal plates are arranged as in a staircase and each is aligned parallel to the surface. A cross-sectional view of the test pit is provided in Fig. (3). The GPR system is dragged over the targets and data taken at 166 uniformly spaced positions over the targets, so 166×128 complex values of data are recorded for the run. To form the image, an inverse FFT is performed on each of the columns and stored. To compensate for the attenuation of the return signal at greater depths, the magnitude of the output image is multiplied by the depth-dependent function r^2. The compensated image is displayed in Fig. (4). This image is the most basic image formed by the step-chirp radar system.

Enhancement technique

The stepped chirp system, at each spatial position, receives N complex returns at N frequencies of transmission. When a single target is present, the data is in the form of:

$$v(n) = A_n\, e^{-j\phi n}, \quad 0 \le n \le N-1 \tag{15}$$

where ϕ is a constant dependent on the depth of the target. An FFT of $v(n)$ provides the range profile at this position. Performing FFT's at multiple positions forms images such as Fig. (4), where 7 metal plates 1–7 ft. deep are displayed. In the calculation of each inverse FFT, each point in the range profile is formed by summing each of the N complex returns multiplied by phase terms which are dependent on the depth of the point in the range profile. The range profile of a single column is given by:

$$\begin{aligned} V(k) &= \frac{1}{N}\sum_{n=0}^{N-1} v(n)e^{j\frac{2\pi k}{N}n} \\ &= \frac{1}{N}\sum_{n=0}^{N-1} A_n e^{j\left(\frac{2\pi k}{N}-\phi\right)n} \\ &= \frac{1}{N}\sum_{n=0}^{N-1} s(k,n), \quad 0 \le k \le N-1 \end{aligned} \tag{16}$$

where $s(k,n) = A_n e^{j\left(\frac{2\pi k}{N}-\phi\right)n}$ forms the wavefield of $V(k)$ and k is the depth index. The enhancement technique is based on the statistics of the wavefield terms in the summation of $V(k)$. Let us observe the terms in the sum of Col. 62 of Fig. (4) where a target is present at depth index $k = 52$. In Fig. (5), the phases of the terms in the sum of $V(k)$ are displayed at $k = 15$, a depth far from the target where $\frac{2\pi k}{N} \ll \phi$. As n goes from to $N-1$, the product

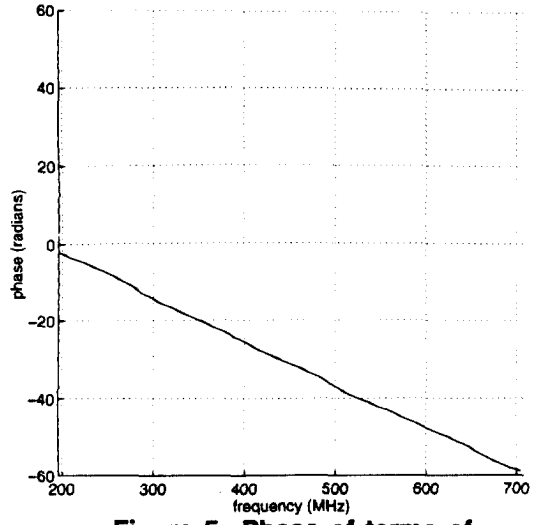

Figure 5. Phase of terms of $V(k)$, Column 62, depth $k = 15$.

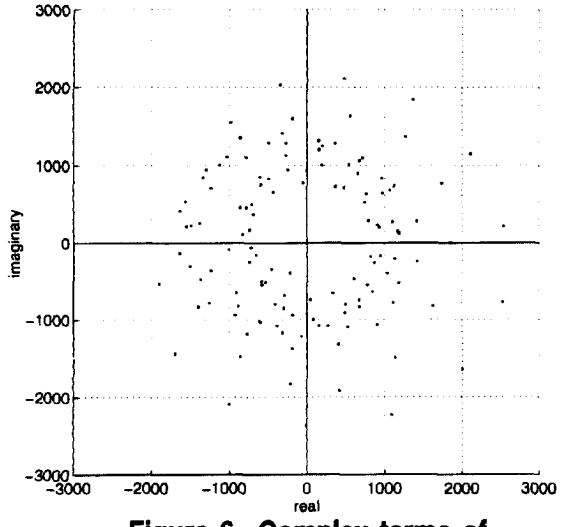

Figure 6. Complex terms of $V(k)$, Column 62, depth $k = 15$.

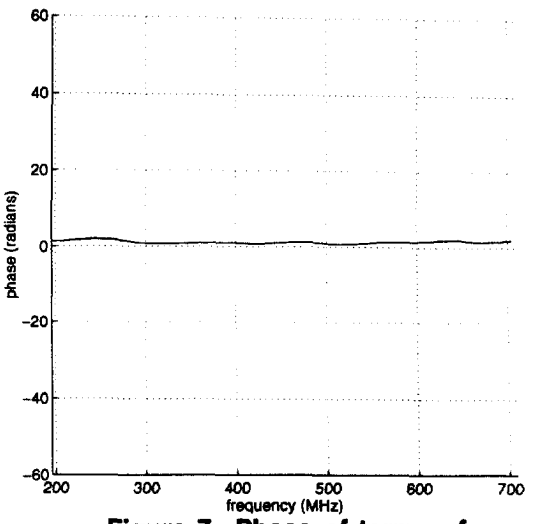

Figure 7. Phase of terms of $V(k)$, Column 62, depth $k = 52$.

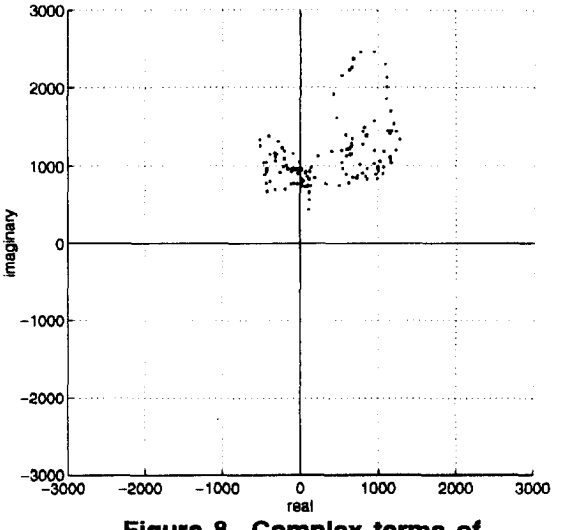

Figure 8. Complex terms of $V(k)$, Column 62, depth $k = 52$.

$\left(\frac{2\pi k}{N} - \phi\right) \times n$ gives a wide range of phases and the terms of $V(k)$ are roughly uniformly spread over the complex plane, as shown by Fig. (6). The result is the average (the centroid) of these points, and thus $V(k)$, are close to the origin and have a small magnitude. However, when we reach the depth such that $\frac{2\pi k}{N} \approx \phi$, so $\frac{2\pi k}{N} - \phi \approx 0$, k has reached the target at $k = 52$, and the wavefield phases are relatively flat, as shown in Fig. (7). Correspondingly, the terms in the sum of $V(k)$ converge together, as shown in Fig. (8). Thus, when the terms are averaged, there is no canceling of terms and a peak in the magnitude of the range profile forms, indicating the presence of a target at that position. As k moves to depths past the target, we find $\frac{2\pi k}{N} \gg \phi$ and the wavefield terms redistribute themselves uniformly in the complex plane again, with the difference that the phases now have a positive slope with respect to frequency. The key observation is that the variance of the terms, and thus also the standard deviation of the terms, is minimized where a target is present. The standard deviation is computed by:

$$\sigma_k = \sqrt{\frac{1}{N}\sum_{n=0}^{N-1}\left(s(k,n) - \overline{s}\right)^2}$$

$$= \sqrt{\frac{1}{N}\sum_{n=0}^{N-1}\left(v(n)e^{j\frac{2\pi k}{N}n} - V(k)\right)^2},$$

$$0 \le k \le N-1 \qquad (17)$$

where $\overline{s}$ is the average of all the $s(k,n) = v(n)e^{j\frac{2\pi k}{N}n}$ terms ($\overline{s} = V(k)$). This observation forms the basis for the image enhancement technique, which divides each point

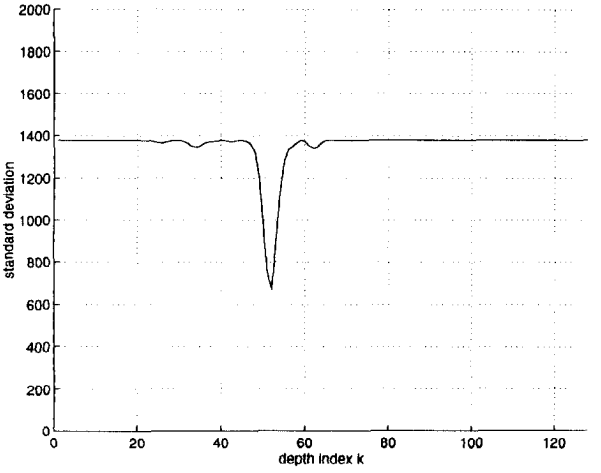

Figure 9. Standard deviation of wavefield terms of $V(k)$ vs. depth, Column 62.

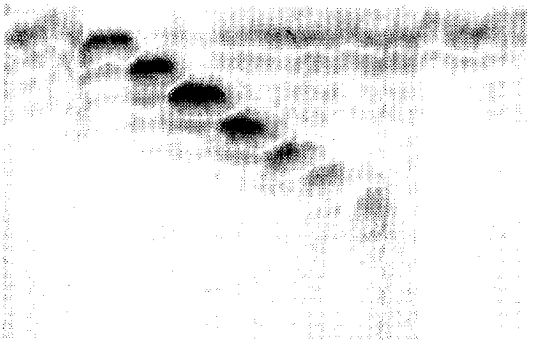

Figure 10. Enhanced image of 7 buried metal plates.

in the image by the standard deviation at each point. The result is that points at targets are normalized by smaller numbers, and points where targets are not present are normalized by larger numbers, enhancing the resolution. If we calculate the standard deviations at the points discussed above, we find the values are minimized at the target at $k = 52$. Fig. (9) displays the standard deviation at each depth in Col. 62. Dividing each point in the image by the standard deviation at the point enhances the target peaks, as shown in Fig. (10), where the image of the 7 metal plates is displayed after enhancement.

Conclusion

We have presented a stepped chirp radar system that has a wide range of subsurface imaging applications. The subsurface radar obtains frequency-domain data and forms a depth profile with Fourier Transforms. An image enhancement technique is introduced which uses the wavefield statistics to clarify the targets in the depth profiles.

Acknowledgment

This research is supported by the National Science Foundation and the National Research Council. Special thanks to Steven Koppenjan and Michael Martinez of Special Technologies Laboratory for supplying the data used for this research project.

References

[1] S. K. Koppenjan and M. B. Bashforth, "Ground penetrating radar applications: Department of energy case studies," *Underground and Obscured Object Imaging and Detection, Del Grande, N., Cindrich, I., and Johnson, P., SPIE Proceedings*, vol. 1942, Apr. 1993.

[2] M. K. Lim and C. A. Olson, "Use of nondestructive impulse radar in evaluating civil engineering structures," *Proceedings of Nondestructive Evaluation of Civil Structures and Materials*, pp. 167–176, 1990.

[3] J. E. Mast, H. Lee, W. C. Chew, and J. P. Murtha, "Pulse-echo holographic techniques for microwave subsurface nde," *Proceedings of Nondestructive Evaluation of Civil Structures and Materials*, pp. 177–191, 1990.

[4] S. K. Koppenjan and M. B. Bashforth, "The department of energy's ground penetrating radar (gpr), an fm-cw system," *Underground and Obscured Object Imaging and Detection, Del Grande, N., Cindrich, I., and Johnson, P., SPIE Proceedings*, vol. 1942, Apr. 1993.